Influence of Quenching Treatments on Structure and Conductivity of the $Li_{3x}La_{2/3-x}TiO_3$ Series

A. Várez,*[,†] J. Ibarra,[†,#] A. Rivera,[‡,||] C. León,[‡] J. Santamaría,[‡] M. A. Laguna,[§] M. L. Sanjuán,[§] and J. Sanz[||]

Dpto. Ciencia de Materiales, Universidad Carlos III de Madrid, 28911 Leganés, Madrid, Spain, Dpto. Física Aplicada III, Universidad Complutense, 28040 Madrid, Spain, Inst. Ciencia de Materiales de Aragón, Universidad de Zaragoza-CSIC, Facultad de Ciencias, 50009 Zaragoza, Spain, and Inst. Ciencia de Materiales de Madrid, CSIC, Cantoblanco, 28049 Madrid, Spain

Received April 4, 2002. Revised Manuscript Received October 21, 2002

The effect of high-temperature treatments on the structure and lithium mobility of the $Li_{3x}La_{2/3-x}TiO_3$ ($0.03 \leq x \leq 0.167$) series has been studied by HTXRD, Raman, NMR, and impedance spectroscopies. Room temperature XRD patterns of slowly cooled samples display a **c**-doubled perovskite with orthorhombic or tetragonal symmetries, whereas those of quenched samples display a simple cubic perovskite. However, Raman spectra of analyzed samples are interpreted, in all the cases, with a tetragonal symmetry in which cation disorder increases with the lithium content and quenching treatments. The existence of small microtwinned domains, arranged along the three directions of the perovskite, favors detection of the cubic phase in XRD patterns. From ^{7}Li NMR spectroscopy a two-dimensional Li motion was detected in ordered samples, which becomes progressively three-dimensional as cation disordering increases. The presence of microdomains decreases the dc-conductivity of quenched Li-poor samples.

Introduction

The interest in $Li_{3x}La_{2/3-x}TiO_3$ perovskites, $0 < x \leq 0.167$, has considerably increased since the discovery of its high ionic conductivity (i.e., 10^{-3}−10^{-4} Scm^{-1}) reported first by Belous[1] and later by Inaguma et al.[2] This fact makes these materials potential candidates to be used as electrolytes in solid-state batteries, ion-selective membranes, and other electrochemical devices.[3,4] On the basis of these facts, important efforts have been devoted to analyze structural attributes that enhance conductivity in these perovskites such as Li coordination,[5,6] charge carrier mobility,[7−9] structural distortions,[10,11] and vacant sites distribution.[12−14]

In $Li_{3x}La_{2/3-x}TiO_3$ perovskites, La^{3+} ions can be substituted by Li^+ ions, and the number of nominal vacant A sites is given by $= {}^1/_3 - 2x$. Since the discovery of its outstanding electrical properties, several groups have investigated the role played by the vacant sites in the ionic conductivity of these materials. In Li-poor members, the ordering of vacancies is produced in alternate planes along the **c**-axis, like the end member of the series,[15] favoring a two-dimensional conductivity.[16,17] In Li-rich samples, vacancies ordering is removed and conductivity displays a three-dimensional character.[18] To reduce the cation ordering, Harada et al.[19,20] studied the influence of quenching treatments. These studies showed that fast cooling from high-temperature stabilized the cubic phase, mentioned by

* To whom correspondence should be addressed. Phone: +34 91 624 94 84. Fax: +34 91 624 94 30. E-mail: alvar@ing.uc3m.es.
† Universidad Carlos III de Madrid.
‡ Universidad Complutense.
§ Universidad de Zaragoza-CSIC.
|| Inst. Ciencia de Materiales de Madrid, CSIC.
Present address: Fac. Químicas, División de Estudios Superiores, Apdo. Postal 1625, Universidad Autónoma de Nuevo León, 64570 Monterrey, México.

(1) Belous, A. G.; Novitskaya, G. N.; Polyanetskaya, S. V.; Gornikov, Y. I. *Izv. Akad. Nauk SSSR, Neorg. Mater.* **1987**, *23*, 470.
(2) Inaguma, Y.; Chen, L.; Itoh, M.; Nakamura, T.; Uchida, T.; Ikuta, H.; Wakihara, M. *Solid State Commun.* **1993**, *86*, 689.
(3) Colbow, K. M.; Dahn, J. R.; Haering, R. R. *J. Power Sources* **1989**, *26*, 397.
(4) Takahasi, T., Ed. *High Conductivity Solid Ionic Conductor*; World Scientific: Singapore, 1989.
(5) Skakle, J. M. S.; Mother, G. C.; Morales, M.; Smith, R. I.; West, A. R. *J. Mater. Chem.* **1995**, *5*, 1807.
(6) Alonso, J. A.; Sanz, J.; Santamaría, J.; León, C.; Várez, A.; Fernández-Díaz, M. T. *Angew. Chem., Int. Ed.* **2000**, *39* (3), 619.
(7) Emery, J.; Buzare, J. Y.; Bohnke, O.; Fourquet, J. L. *Solid State Ionics* **1997**, *99*, 41.
(8) León, C.; Lucía, M. L.; Santamaría, J.; París, M. A.; Sanz, J.; Várez, A. *Phys. Rev. B* **1996**, *54*, 184.
(9) León, C.; Rivera, A.; Várez, A.; Sanz, J. Santamaría, J.; Ngai, K. L. *Phys. Rev. Lett.* **2001**, *86*, 1279.
(10) Sanz, J.; Alonso, J. A.; Várez, A.; Fernández-Díaz, M. T. *J. Chem. Soc., Dalton Trans.* **2002**, 1406.
(11) Fourquet, J. L.; Duroy, H.; Crosnier-López, M. P. *J. Solid State Chem.* **1996**, *127*, 283.
(12) Kawai, H.; Kuwano, J. *J. Electrochem. Soc.* **1994**, *141*, L78.
(13) Inaguma, Y.; Chen, L.; Itoh, M.; Nakamura, T. *Solid State Ionics* **1994**, *70*, 196.
(14) Inaguma, Y.; Itoh, M. *Solid State Ionics* **1996**, *86*−*88*, 257.
(15) MacEachern, M. J.; Dabkowska, H.; Garrett, J. D.; Amow, G.; Gong, W.; Liu, G.; Greedan, J. E. *Chem. Mater.* **1994**, *6*, 2092.
(16) Paris, M. A.; Sanz, J.; Leon, C.; Santamaría, J.; Ibarra, J.; Varez, A. *Chem. Mater.* **2000**, *12*, 1694.
(17) Ruiz, A. I.; López, M. L.; Veiga, M. L.; Pico, C. *Solid State Ionics* **1998**, *112*, 291.
(18) Ibarra, J.; Várez, A.; León, C.; Santamaría, J.; Torres-Martínez, L. M.; Sanz, J. *Solid State Ionics* **2000**, *134*, 219.
(19) Harada, Y.; Ishigaki, T.; Kawai, H.; Kuwano, J. *Solid State Ionics* **1998**, *108*, 407.
(20) Harada, Y.; Hiracoso, Y.; Kawai, H.; Kuwano, J. *Solid State Ionics* **1999**, *121*, 245.

10.1021/cm020172q CCC: $25.00 © 2003 American Chemical Society
Published on Web 12/07/2002

Robertson et al,[21] where vacant sites are completely disordered. However, this treatment produced the opposite effect on the conductivity of samples with high and low Li content; dc-conductivity increased in the first case but decreased in the second one.

To better assess the influence of the vacancies distribution on the conductivity of the $Li_{3x}La_{2/3-x}TiO_3$ series, we have analyzed the effect of quenching treatment in perovskites with different Li content. Moreover, we have studied, by means of high-temperature X-ray diffraction experiments, the expansion and the possible cation disordering produced during the heating of samples. To get insight into the local structure of these samples, Raman experiments have been performed. Finally, local and long-range mobility of lithium has been studied by NMR and electrical impedance techniques.

Experimental Section

$Li_{3x}La_{2/3-x}TiO_3$ samples with different x values ($0.03 \leq x \leq 0.167$) were synthesized by solid-state reaction of stoichiometric amounts of dried Li_2CO_3, La_2O_3, and TiO_2 using dense alumina crucibles and following the procedure used in a previous work.[18] Synthesized powders were finely ground in acetone using an agate ball mill and then cold pressed into pellets (13-mm diam., 1−2 mm thick) at 200 MPa; afterward, pellets were heated at 1573 K during 6 h. From this temperature, samples were either quenched into liquid nitrogen (Q samples) or slowly cooled (1 °/min) to room temperature (SC samples).

X-ray diffraction (XRD) experiments were carried out on a Philips X'Pert-MPD automatic diffractometer ($\theta/2\theta$ Bragg−Brentano geometry) with Cu Kα radiation working at 40 kV and 50 mA. The experimental conditions were the following: 2θ range of 10−90° in a step-scanning mode (0.02° step); 10 s of counting time; divergence slit 1°; anti-scatter slit 1°; and receiving slit 0.1 mm. The Rietveld refinement of the RT-XRD patterns was carried out using the Fullprof program.[22] High-temperature X-ray diffraction (HT-XRD) was used to examine in situ possible structural modifications produced between room temperature and 1573 K. For these measurements, a high-temperature camera (HTK10, Anton PAAR) was used and samples were spread like slurry on the surface of the platinum plate heater. The sample temperature was measured with a Pt−PtRh10% thermocouple welded at the backside of the Pt plate heater. The experiments were carried out, under vacuum atmosphere, in the 2θ range of 10−80° with a step of 0.02° and 4 s of counting time (more the 4 h per XRD-pattern). Lattice parameters were determined by means of the profile-matching facility of the Fullprof software package.[22]

^{7}Li NMR spectra were taken in a MSL 400 Bruker spectrometer working at 155 MHz. Static spectra were taken after irradiation of the sample with a $\pi/2$ pulse (3 μs). The recycling time used between accumulations was 10 s and the number of scans was 100. The filter used during the signal detection was 100 kHz. Chemical shifts of NMR signals were referred to a 1 M LiCl aqueous solution. The fitting of the experimental patterns was carried out using the WINFIT Bruker software. Intensity, position, and line width of components were determined with a nonlinear iterative least-squares method. However, quadrupole C_Q and η constants were determined by a trial and error procedure.

Raman spectra of SC and Q samples with different Li contents were recorded at room temperature in a Dilor XY spectrometer with a diode array detector. Light from an Ar^+ laser at 514.5 nm was focused onto the sample through a 50× microscope objective lens. The power at the sample was ≤10 mW, and the spectral resolution was typically 3 cm^{-1}.

Electrical conductivity measurements were carried out by complex impedance spectroscopy, using automatically controlled HP4284A and HP4285A precision LCR meters in the frequency range 20 Hz to 30 MHz. The temperature range was 150−500 K. All measurements were performed on cylindrical pellets (5 mm diam. and 0.7 mm thick) with evaporated gold electrodes, under a dry N_2 flow to insure an inert atmosphere. dc-conductivity values (σ_{dc}) were obtained from the fit of the real part of the conductivity to the universal response $\sigma' = \sigma_{dc}(1 + (\omega/\omega_p)^n)$ as described elsewhere.[8]

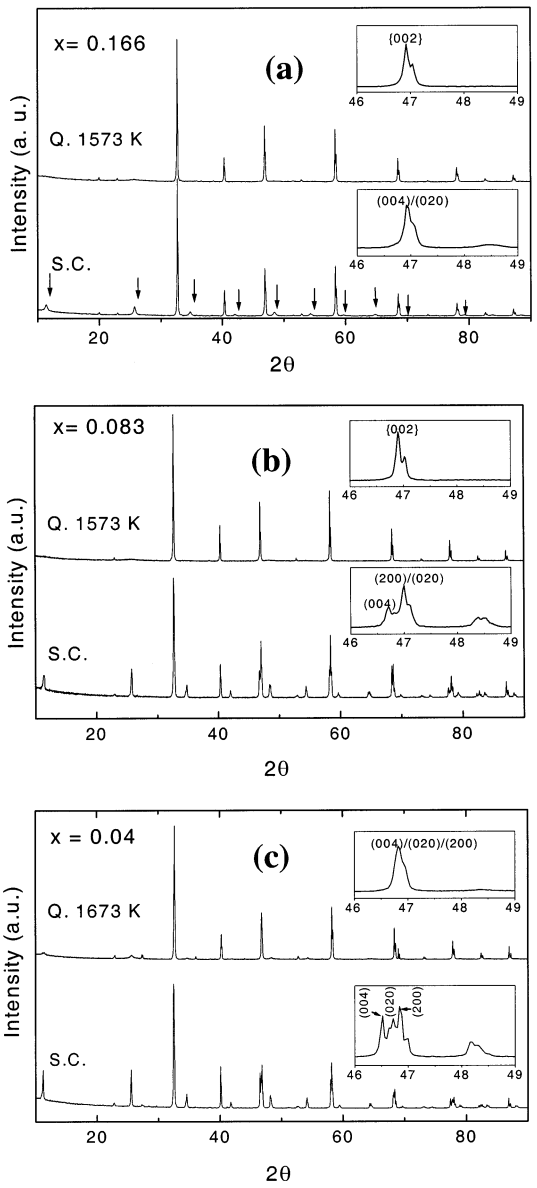

Figure 1. Powder X-ray diffraction patterns of slowly cooled (SC) and quenched (Q) samples. A magnification of $46 \leq 2\theta \leq 49$ region illustrates changes produced on symmetry. Arrows in the top of the plot denote superstructure peaks associated with doubled perovskites.

Results

X-ray Diffraction. *Quenching Treatments.* In Figure 1 the effect of quenching treatments on XRD patterns of $Li_{3x}La_{2/3-x}TiO_3$ samples, with $x = 0.04$, 0.083, and 0.167, is shown. For high lithium contents a change of

(21) Robertson, A. D.; García-Martín, S.; Coats, A.; West, A. R. *J. Mater. Chem* **1995**, *5*, 1405.

(22) Rodríguez-Carvajal, J. *Phys. B* **1992**, *192*, 55. (Fullprof Program: Rietveld Pattern Matching Analysis of Powder Patterns, Grenoble, ILL, 1990).

symmetry from tetragonal ($a_p \times a_p \times 2a_p$; space group $P4/mmm$) to cubic was observed when the sample was quenched into liquid N_2 from 1573 K (Figure 1a). In agreement with data reported by Harada et al.,[20] superstructure peaks associated with the **c**-axis doubling (arrows of Figure 1a) disappeared after this treatment. XRD patterns of quenched samples were indexed with a cubic cell ($a_p \approx 3.872$ Å; space group $Pm3m$).

For intermediate compositions ($x = 0.083$) the behavior is quite similar to that described for high Li contents. However, in slowly cooled tetragonal samples ($a_p \times a_p \times 2a_p$; space group $P4/mmm$) the measured $c/2a$ ratio is clearly higher, as deduced from the separation between (004) and (020)/(200) peaks at $2\theta \approx 47°$ (inset of Figure 1b). In quenched samples from 1573 K this separation disappears and the unit cell becomes again cubic ($a_p \approx 3.877$ Å).

In the case of the slowly cooled samples with low lithium content ($x = 0.04$), XRD patterns were fitted with an orthorhombic **c**-axis doubled unit cell ($a_p \times a_p \times 2a_p$; space group $Pmmm$). The orthorhombic distortion is clearly observed in the $2\theta \approx 47°$ region, where (004), (020), and (200) peaks were differentiated (inset of Figure 1c). Orthorhombic samples display a $c/2a^*$ ratio >1, with a^* standing for the average of a and b parameters. When samples were quenched from 1573 K into liquid nitrogen, the number of peaks decreased in XRD patterns, and characteristic peaks of the orthorhombic distortion merged into single peaks, indicating the formation of the cubic phase ($a_p \approx 3.879$ Å). However, in this case, superstructure peaks did not disappear completely from XRD patterns, even in samples quenched from 1673 K. In samples heated for long times at 1673 K, small peaks were detected at $2\theta \approx 27.4°$ and 36°, which increased with the extent of the thermal treatments. These peaks correspond to the most intense reflections of the $La_2Ti_2O_7$ compound. The presence of this phase is probably due to prolonged annealing at high temperature producing Li_2O loss, and shifting the composition to the biphasic region of the phase diagram.[21]

High-Temperature XRD. To confirm structural modifications produced at high temperatures, slowly cooled samples with high, intermediate, and low lithium contents were analyzed as a function of temperature. Figure 2 shows the temperature evolution of some of XRD patterns of the orthorhombic sample, $x = 0.04$, illustrating the evolution of the (004), (020), and (200) peaks (insets of the figure). Below 773 K, (020) and (200) peaks remain split, but merge into a single one at 773 K as a consequence of the orthorhombic to tetragonal transformation.[16] An appreciable disordering was detected between 773 and 1573 K; however, superstructure peaks do not completely disappear, indicating that the **c**-axis doubling remains even at 1573 K. As the temperature increases, peaks shift toward lower angles according to the unit cell thermal expansion.

In the case of the tetragonal perovskite ($x = 0.083$), heating of the sample above 1373 K produces an attenuation of the intensity of superstructure peaks (Figure 3); in particular, the peak located at $2\theta \approx 11°$ disappears at 1473 K. The progressive overlapping of the (114) and (122) peaks (inset of Figure 3) indicates

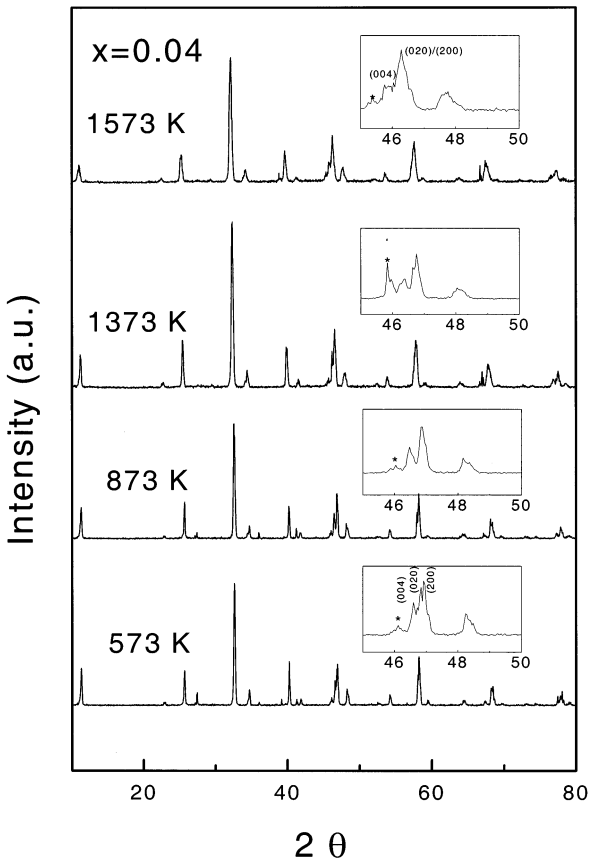

Figure 2. Powder XRD patterns of low Li content samples, $x = 0.04$, at increasing temperatures. The convergence of the (020) and (200) peaks at 47° (see inset) illustrate the orthorhombic−tetragonal transformation. The Pt peaks of the holder are labeled with an asterisk.

the continuous decrease of the $c/2a$ ratio with the temperature.

The XRD pattern of the lithium-rich samples ($x = 0.167$) is similar to that of tetragonal ones; however, no splitting of the (004) and (020)/(200) peaks was detected (Figure 4). The intensity of superstructure peaks decreased above 1073 K, but they do not completely disappear at high temperature except in the case of the peak at $2\theta \approx 11°$. In quenched samples, heating of the perovskites only produced the peak shift associated with the unit cell expansion.

^{7}Li NMR Spectroscopy. ^{7}Li ($I = 3/2$) NMR spectra of the three analyzed samples are formed by three components associated with the central transition ($-1/2 \rightarrow 1/2$) and the two satellite transitions ($-3/2 \rightarrow -1/2$; $1/2 \rightarrow 3/2$). In all cases, intensity of the central line was considerably higher than that expected for a single distorted site, indicating that spectra are formed by two components with different mobility.

In analyzed perovskites, mobile species are responsible for the intense narrow central line, and fixed species caused the detection of satellite transitions (Figure 5). Quadrupolar constants (C_Q) of the two species are respectively $C_{Q1} \leq 10$ kHz and $C_{Q2} = 100$ kHz. The intensity of satellite transitions decreases with the amount of lithium and with quenching treatments. In quenched samples, a broadening of the baseline of the NMR line is detected which has been ascribed to residual quadrupole interactions. In the quenched cubic $Li_{0.5}La_{0.5}TiO_3$ sample, the intensity of satellite lines is

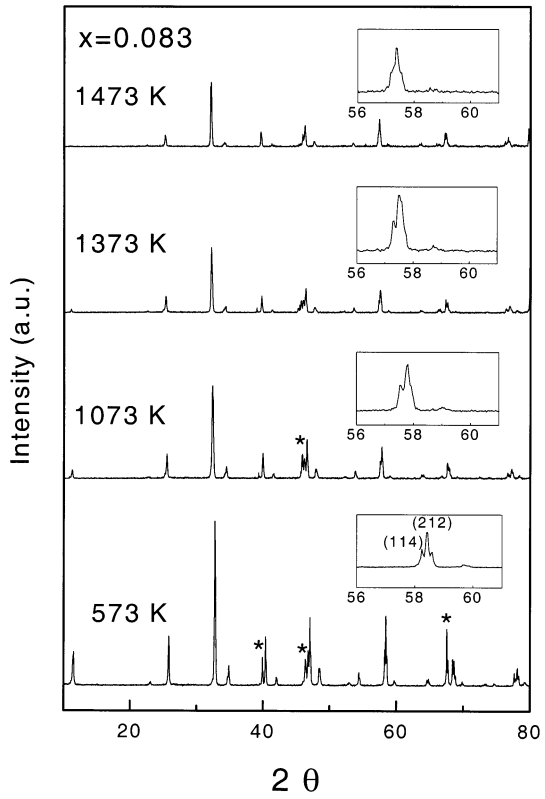

Figure 3. High-temperature XRD patterns for intermediate Li content samples ($x = 0.083$). Insets display the evolution of (114) and (212) reflections with temperature.

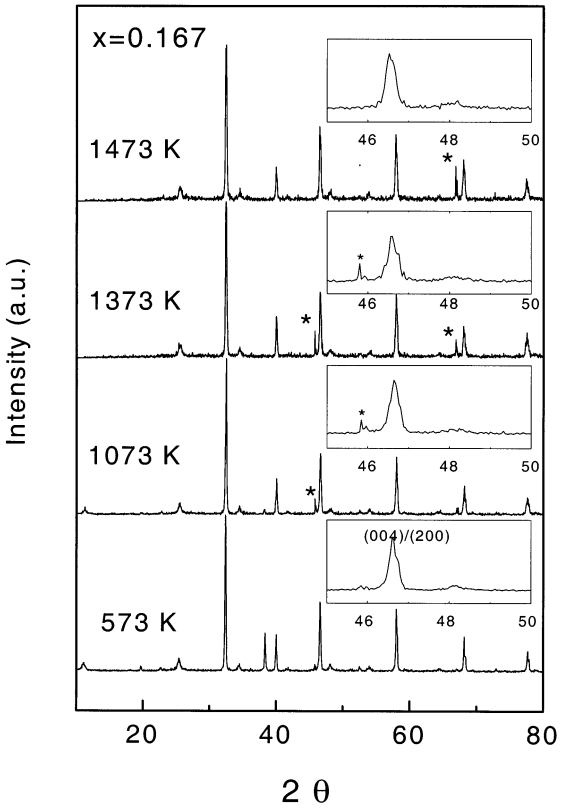

Figure 4. Evolution of the XRD patterns with the temperature for high Li content samples ($x = 0.167$). Insets ilustrate the convergence of (004) and (200) peaks with temperature.

very low and the line-width of the central transition is very small, indicating that most of lithium displays high mobility.

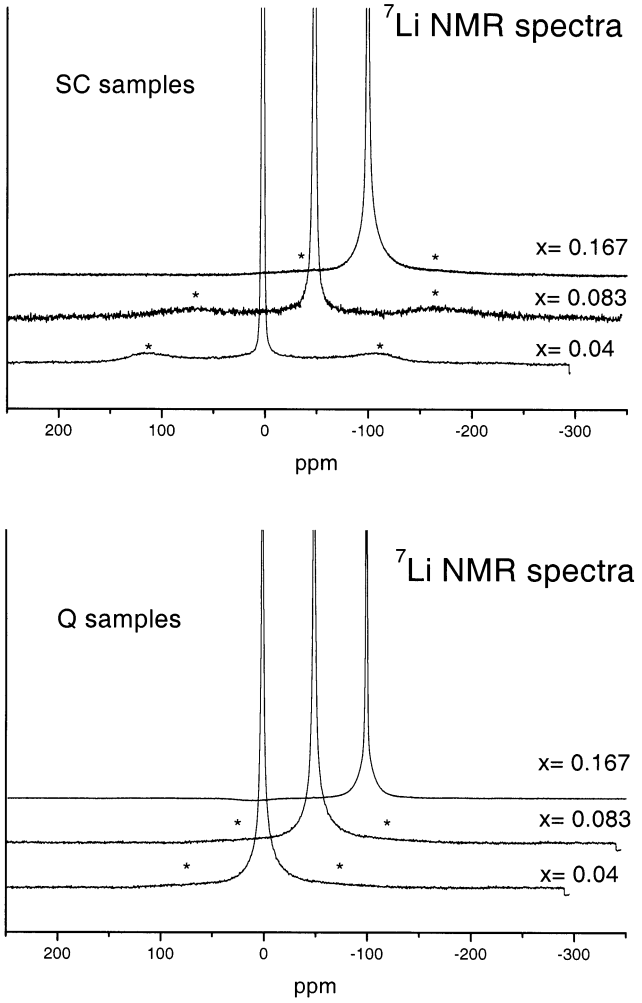

Figure 5. ^{7}Li NMR spectra recorded at room temperature for slowly cooled (SC) and quenched (Q) samples of three analyzed compositions. The intensity of quadrupole outer transitions (marked as asterisks) decreases with the Li content and with quenching treatments.

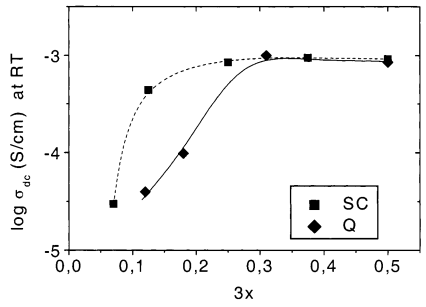

Figure 6. Bulk ionic dc-conductivity measured at room temperature in quenched and slowly cooled samples.

Li Ion Conductivity. Figure 6 shows dc-conductivities at room temperature versus lithium content of quenched and slowly cooled samples. The σ_{dc} increases with lithium content, reaching in both types of samples a plateau at $x = 0.1$. For Li-rich samples quenching treatments do not appreciably modify dc-conductivity values, but for Li-poor samples the conductivity was found to decrease with this treatment almost one order of magnitude. The lower values of σ_{dc} measured in Li-poor samples cannot be ascribed to differences in activation energies for Li diffusion and have been attributed to variations in the preexponential factor of

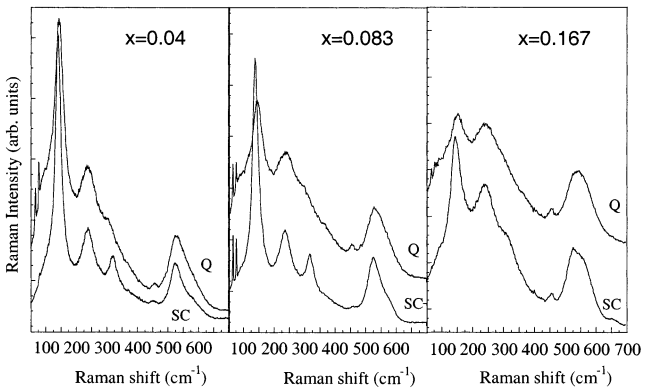

Figure 7. RT Raman spectra of slowly cooled (SC) and quenched (Q) samples with different lithium contents.

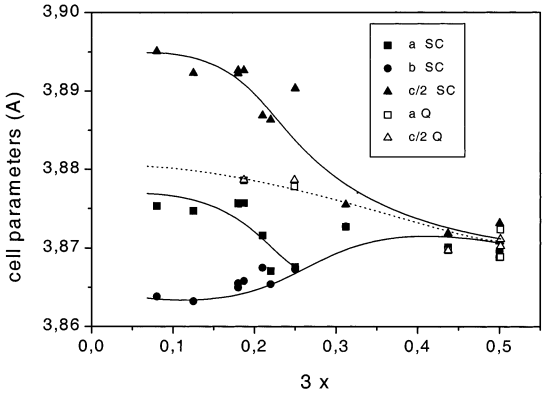

Figure 8. Evolution of cell parameters with the Li content for slowly cooled (closed symbols) and quenched samples (open symbols). XRD patterns of quenched samples were indexed with a cubic unit cell.

the conductivity. In particular the observed variation has been previously ascribed to the evolution of charge carrier concentrations.[18]

The dc-conductivities of samples display a non-Arrhenius behavior with the inverse of temperature. In all cases apparent activation energies, defined as the slopes of σ_{dc} conductivity data in Arrhenius plots, are found to decrease from 0.40 ± 0.02 to 0.28 ± 0.02 eV with increasing temperatures.[8,18]

Raman Spectroscopy. Figure 7 shows the room temperature Raman spectra of $x = 0.04$, 0.083, and 0.167 compounds both slowly cooled (SC; lower graphs) and quenched from high temperature (Q; upper graphs). The most remarkable effects of quenching treatments on the spectra are the general broadening of all observed features and the change in intensity of some of these features, either decreasing (such as the peak at about 320 cm^{-1}) or increasing (peak close to 450 cm^{-1}). Despite these differences, spectra of quenched samples look quite similar to those of SC samples. According to our previous interpretation,[23] these spectra can be explained by assuming a tetragonal structure, at least in a scale of several unit cells. Small changes detected along the series have been mainly ascribed to cation disorder which increases when the lithium content increases or with quenching treatments.

Discussion

Perovskite Structure. Unit cell parameters of slowly cooled $Li_{3x}La_{2/3-x}TiO_3$ perovskites are given in Figure 8. As it is well established, the La and vacancies ordering in alternating planes of the perovskite produces the **c**-axis doubling. Two different features are produced when the Li content increases: the vacancies are progressively disordered and the $c/2a$ ratio decreases. In ordered Li-poor samples ($x < 0.08$) an orthorhombic distortion (space group $Pmmm$), scarcely reported in previous works, is detected, and the $c/2a$ ratio is higher than 1.[16] For Li-rich samples ($x > 0.1$), the XRD patterns were interpreted assuming a tetragonal symmetry (space group $P4/mmm$), with a $c/2a$ parameter near 1.[18] In the last samples, superstructure peaks are broad, indicating the presence of a considerable disorder.

The c/*a* enlargement in Li-poor samples is associated with a displacement of the Ti ions along the **c**-axis, produced to compensate the asymmetric distribution of charges around octahedra.[11,18] Ti displacements produce the sequence of long−short−short−long Ti−O bond distances along the **c**-axis that preclude the appearance of a macroscopic electrical polarization. When the Li content increases, the vacancies ordering is progressively eliminated and the octahedra become regular. As a consequence of this fact the $c/2a$ ratio tends to 1.[11,12,18]

In quenched samples, XRD patterns display the quasi-cubic symmetry, suggesting that an important disordering of cations in A sites of the perovskite is produced.[19,20] From the analysis of Figure 8, it can be deduced that for a given composition the unit cell volume does not change appreciably with quenching treatments, but decreases with the Li content of the sample. This observation is in agreement with the different radii of La and Li cations.

To improve cation disorder, La ions must pass through square windows defined by every four corner-sharing octahedra. From a structural point of view, and considering a rigid sphere model with Shannon radii,[24] La ion diffusion is unlikely to occur even at high temperature because square windows, with a diagonal O−O ≈ 3.9 Å, are considerably smaller than the La ionic size, 2(La−O) = 5.46 Å. However, some diffusion of La assisted by oxygen motion cannot be disregarded at high temperatures. Acording to the above facts, Harada et al.[20] suggested that La diffusion starts at 600 °C, but requires high temperatures (1423 K) or long annealing times (more than one week) to modify the starting distribution. Similar observations have been found in this work: XRD patterns of quenched samples display the cubic symmetry; however, in the case of slowly cooled Li-poor samples, small superstructure peaks remain after long annealing times at high temperature.

Perovskite Thermal Expansion. The evolution of unit cell parameters with the temperature is given in Figure 9. For samples with low lithium contents ($x = 0.04$), an orthorhombic−tetragonal transition is observed at temperatures near 773 K.[16] However, no more transformations were detected in the 873−1573 K temperature range. Up to 873 K the lattice parameters increase smoothly with temperature, whereas for higher temperatures the expansion becomes more important.

(23) Sanjuán, M. L.; Laguna, M. A. *Phys. Rev. B* **2001**, *64*, 174305.

(24) Shannon, R.D. *Acta Crystallogr. A* **1976**, *32*, 751.

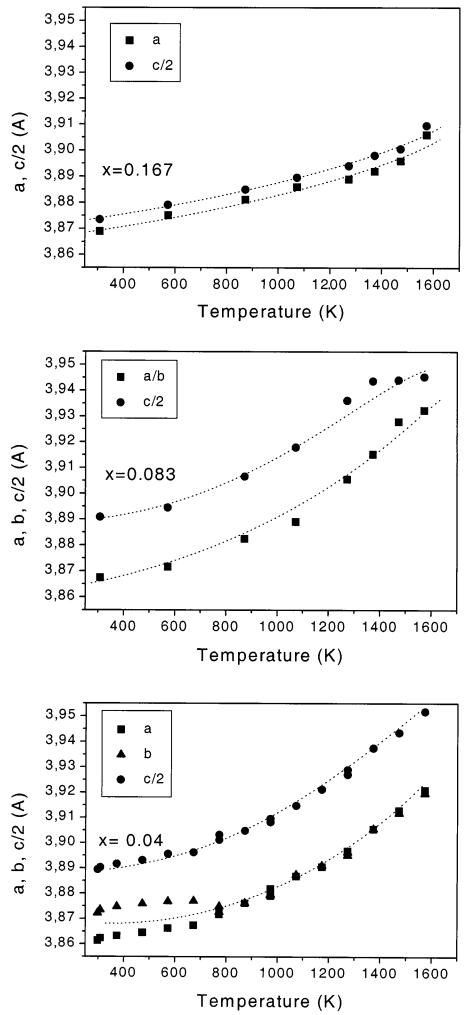

Figure 9. Lattice parameters (Å) versus temperature (K) for slowly cooled samples with three different Li contents.

In the temperature range analyzed, differences between **a** and **c** parameters remain constant.

In the case of samples with $x = 0.083$, two regimes were identified between room temperature and 1400 K. Up to 873 K the thermal expansion of the unit cell is small; however, from 873 to 1400 K the expansion of the unit cell increases considerably in the same way as that sample with $x = 0.04$. However, at higher temperatures a new regime could be present in which the c/a ratio decreased, suggesting that vacancies become progressively disordered.

For the lithium-rich sample, $x = 0.167$, the thermal expansion is quite isotropic and both tetragonal unit cell parameters follow similar trends. In these perovskites the total expansion measured at 1573 K is lower than that in other compositions.

To analyze the thermal expansion of samples, the measured lattice parameters were fitted to the relations[25]

$$a(T) = a_0 + a_1T + a_2T^2$$

$$c(T) = c_0 + c_1T + c_2T^2$$

where $a(T)$ and $c(T)$ are the lattice parameters measured at the temperature T. The results of this analysis are listed in Table 1. Linear thermal expansion coefficients (α) were calculated according to the expression[25]

$$\alpha(T) = \frac{1}{a_{298}} \frac{da_T}{dT}$$

where a_T and a_{298} stand for lattice parameters measured at T and 298 K, respectively. Calculated results are plotted versus temperature in Figure 10. In all cases, thermal expansion increases almost linearly with temperature. In Li-rich samples, $x = 0.167$, unit cell expansions are small and isotropic; however, in Li-poor samples, $x = 0.04$, thermal expansions are more important and preserve the axial symmetry. Finally, in intermediate compositions, thermal expansions are different along the two axes: the expansion coefficient of the **c**-axis is smaller than that of the **a**-axis at low temperature; however, the contrary is produced at high temperatures. This fact allows the **c** and **a** parameters to approach to a common value.

Cation Disordering. To analyze the distribution of vacancies in perovskites, we have performed the Rietveld analysis of the HTXRD patterns, assuming the existence of two sites for La ions in tetragonal and orthorhombic phases.[11,16−18] In Li-poor samples, the occupation of the two sites was very different in the whole temperature range analyzed (RT−1573 K). In the case of intermediate compositions, occupation of these sites becomes similar at increasing temperatures. Finally, in Li-rich samples, the occupation of both sites is very close in all temperatures analyzed. However, agreement factors obtained in Rietveld analysis are not good because of the coexistence of broad and narrow peaks in XRD patterns. This analysis suggests that the structural models considered here are not adequate to describe structural features of perovskites, and more elaborated models, taking into account the structural disordering, are required. The analysis of this point is out of the scope of this work; in consequence, only unit cell parameters of perovskites will be discussed herein.

When cation disordering is produced, superstructure peaks disappear. According to these observations, in Li-rich samples the $c/2a$ ratio is near 1 and does not change very much during sample heating (Figure 11). However, in Li-poor samples this parameter is higher than 1 and increases slightly with temperature. In intermediate compositions, this parameter increases with temperature up to 1273 K, but decreases above this temperature, indicating the progressive coalescence of **a** and **c** parameters associated with the onset of vacancies disordering.

From the structural analysis carried out in this work, it can be deduced that cation disordering is favored by increasing the Li content or by heating samples at high temperatures. In the case of high Li contents, some disorder is produced at 1273 K; however, for low Li contents, temperatures higher than 1573 K are required. In all analyzed perovskites, superstructure peaks cannot be completely eliminated during sample heating, which indicates that cation disordering is very difficult to achieve. Prolonged treatments at 1673 K produce decomposition of starting orthorhombic Li-poor

(25) Yashima, M.; Ali, R.; Yoshioka, H. *Solid State Ionics* **2000**, *128*, 105.

Table 1. Regression Data for $Li_{3x}La_{2/3-x}TiO_3$ Samples, Considering Three Terms in Expressions Describing Lattice Parameter Expansion

x	a_0 (A)	a_1*10^6	a_2 *10^8	R	Sd	c_0	c_1*10^5	c_2*10^8	R	Sd
0.03	3.874(2)	−29 (4)	4 (20)	0.995	0.001	7.78(1)	−2 (60)	6 (32)	0.997	0.002
0.083	3.873(5)	−27 (12)	4 (61)	0.993	0.003	7.76(2)	4 (5)	3.3 (2.4)	0.968	0.010
0.167	3.868(5)	36 (13)	1 (66)	0.962	0.003	7.75(1)	42 (2)	2.5 (95)	0.981	0.004

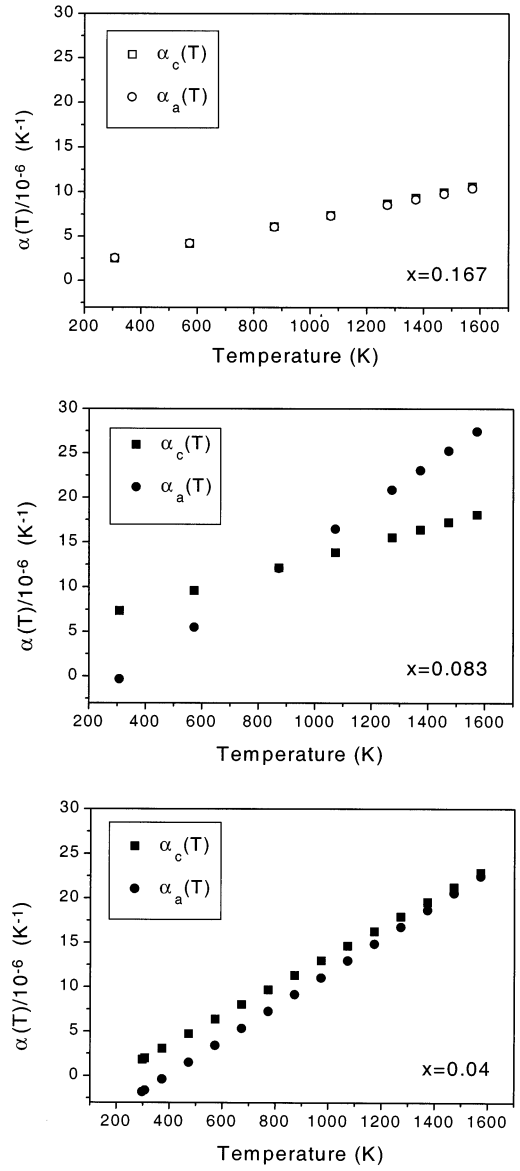

Figure 10. Plot of thermal expansion coefficients (α) versus temperature for three analyzed compositions.

samples. According to this fact, small peaks of $La_2Ti_2O_7$ were detected, which increased with temperature, suggesting some lithia loss during the sample heating. Similar findings were reported in the ideal member, $La_{2/3}TiO_3$,[26] and in $La_{0.683}Ti_{0.95}Al_{0.05}O_3$[27] perovskites, where a small amount of Ti was substituted by Al.

Quenching from high temperature produces a considerable decrease of the superstructure peaks, suggesting that the cation disorder produced is important (Figure 1). These results differ from those obtained by heating the samples up to 1573 K in the HTXRD

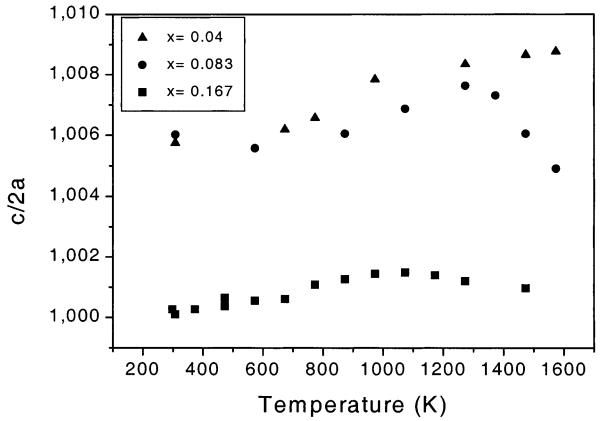

Figure 11. Evolution of the $c/2a$ ratio with the temperature for three different compositions.

chamber, where the cation disordering attained was much lower. To understand these contradictory results, it must be noted that the HREM study of these perovskites showed a microdomain texture, in which the **c**-axes of tetragonal domains were oriented along the three axes of the perovskite.[11,28] Along the series, the size of domains decreases from one hundred to tens of Å[11] as the lithium content increases; from this fact, it is probable that, below a critical size of domains, the XRD technique averages the symmetry of microtwinned regions, favoring detection of the cubic symmetry in quenched samples. Similar effects have been found in other materials (i.e., leucite cubic−tetragonal transformation),[29] where formation of microtwinned domains was produced in order to reduce local strains associated with structural transformations. In these cases, a more local technique is required to analyze the symmetry of these compounds. At this respect, Raman experiments show in all samples analyzed that some cation ordering is always preserved along the series even in quenched samples. On the basis of the above considerations, the broadening of the spectrum and the observed intensity changes can be attributed to either cation disorder or to twinning domain formation. Only in slowly cooled lithium-poor samples, where the size of domain is important, or in quenched lithium-rich samples, where the disorder is maximum, does the structural analysis have a clear significance. In intermediate compositions different degrees of cation order can be obtained depending on thermal treatments used. From the above results we can conclude that most of the cation disorder produced in analyzed perovskites is associated with the incorporation of Li, but some disordering could be produced by microstructure changes induced during quenching treatments. An analysis of the relative contribution of the two effects is difficult.

(26) Abe, M.; Uchino, K. *Mater. Res. Bull.* **1974**, *9*, 147.
(27) Minato, K.; Takano, M.; Fukluda, K.; Sato, S.; Ohashi, H. *J. Alloys Compd*. **1997**, *225*, 18.
(28) Várez, A.; García-Alvarado, F.; Morán, E.; Alario-Franco, M. A. *J. Solid State Chem*. **1995**, *118*, 78.
(29) Palmer, D. C.; Putnis, A.; Salje, E. *Phys. Chem. Miner.* **1988**, *16*, 298.

Li Mobility in Perovskites. As we have recently reported, neutron diffraction experiments showed that for quenched Li-rich samples, Li ions are located at the center of square windows that connect contiguous A-sites of the perovskite.[6] According to geometrical considerations, the square windows size (diagonal distance = 3.9 Å) in these perovskites is near 2(Li−O) ∼ 4.0 Å and a small expansion of the unit cell could substantially enhance the Li mobility.

The study of local mobility by NMR technique showed the existence of two components in the spectra that were ascribed to lithium ions with different mobilities. In **c**-doubled perovskites, the narrow and intense component centered at the resonance frequency was assigned to mobile Li^+ species located at planes with an important amount of vacancies, and the component with satellite transitions was associated with less mobile Li ions located at La-rich planes (Figure 5). From this fact, Li mobility displays a two-dimensional regime[16,17] in ordered samples, but becomes a progressive three-dimensional mobility in disordered samples. Exchange processes between the two planes considerably reduce the amount of fixed ions. In quenched Li-rich samples, vacancies disorder is maximum, and only one type of site is detected.

Along the series, the environment of lithium and activation energies does not change appreciably. From this fact, the increase of σ_{dc} with the Li content has been attributed to changes on the charge carrier concentrations. However, on the basis of the random distribution of vacancies and lithium cations on A-sites of the perovskite, a maximum at $x = 0.08$ should be observed. Moreover, high conductivity values measured in Li-rich samples can only be explained on the basis of the results obtained in neutron diffraction experiments of quenched Li-rich samples.[6] The occupation of the center of unit cell faces by lithium increased the amount of vacant A-sites that participated in the Li conduction. From this fact, the number of vacancies is considerably higher than that deduced from nominal compositions, increasing from 0.33 to 0.5 when the lithium content increases. This explains the increase of conductivity detected along the series.

On the other hand, dc-conductivity of quenched samples displays contradictory results: conductivity of quenched Li-rich samples is slightly higher than that of slowly cooled samples, but in Li-poor samples conductivity decreases, almost by a factor of 10, with this treatment. These results are difficult to understand on the bases of NMR data, where quenching treatments always enhanced the mobility of Li. However, in quenched samples the size of microdomains is reduced and the number of microtwinned domains increases, hindering the long-range motion of lithium. This fact explains the observed decrease in the long-range conductivity. In the case of Li-rich samples, cation disorder is important, and quenching treatment does not appreciably affect the microdomains size; consequently, the conductivity of samples does not change significantly with thermal treatments.

Conclusions

The influence of thermal treatments on the structure and lithium mobility of the series $Li_{3x}La_{2/3-x}TiO_3$ has been analyzed by XRD, Raman, NMR, and impedance spectroscopy. In slowly cooled Li-poor perovskites, $x < 0.08$, cation vacancies are disposed in alternate planes along the **c**-axis, favoring a two-dimensional conductivity along **ab**-planes. In Li-rich samples, $x > 0.08$, cation disorder increases and lithium mobility becomes three-dimensional. In the last cases, the $c/2a$ ratio approaches 1. The unit cell expansion is important in ordered low lithium content samples but decreases when the lithium content increases.

XRD experiments show that symmetry changes from orthorhombic to tetragonal or cubic by quenching treatments or by increasing the Li content. The change of symmetry has often been related to the increase of cation disorder. However, taking into account hindrance of La cations to pass through the square bottlenecks that connect contiguous A-sites of perovskites, detection of cubic symmetry could also be favored by the reduction of the size of microtwinned domains produced during quenching treatments. Tetragonal microdomains will be disposed along the three equivalent directions of the perovskite (microstructural disordering).

The activation energy for Li motion is similar in all samples, indicating that the Li environment does not change along the series. Location of Li at the center of square windows makes the number of vacant A-sites that participate in ionic conduction increase with the substitution of lanthanum by lithium. This fact explains the high conductivity values measured in Li-rich perovskites. From analyzed results, microstructural and structural disorder could have opposite effects on the conductivity of perovskites.

Acknowledgment. We appreciate the financial support of the CICYT (MAT 98-1053-C04 and MAT2001-3713-C04).

CM020172Q